Available online at www.sciencedirect.com

ScienceDirect

Journal of Otology 11 (2016) 165–177

www.journals.elsevier.com/journal-of-otology/

Review

# Inner ear barriers to nanomedicine-augmented drug delivery and imaging☆

Jing Zou [a,b,*], Ilmari Pyykkö [b], Jari Hyttinen [c]

[a] *Department of Otolaryngology – Head and Neck Surgery, Center for Otolaryngology – Head & Neck Surgery of Chinese PLA, Changhai Hospital, Second Military Medical University, Shanghai, China*

[b] *Hearing and Balance Research Unit, Field of Otolaryngology, School of Medicine, University of Tampere, Tampere, Finland*

[c] *Department of Electronics and Communications Engineering, BioMediTech, Tampere University of Technology, Tampere, Finland*

Received 18 October 2016; revised 15 November 2016; accepted 18 November 2016

## Abstract

There are several challenges to inner ear drug delivery and imaging due to the existence of tight biological barriers to the target structure and the dense bone surrounding it. Advances in imaging and nanomedicine may provide knowledge for overcoming the existing limitations to both the diagnosis and treatment of inner ear diseases. Novel techniques have improved the efficacy of drug delivery and targeting to the inner ear, as well as the quality and accuracy of imaging this structure. In this review, we will describe the pathways and biological barriers of the inner ear regarding drug delivery, the beneficial applications and limitations of the imaging techniques available for inner ear research, the behavior of engineered nanomaterials in inner ear applications, and future perspectives for nanomedicine-based inner ear imaging.

Copyright © 2016, PLA General Hospital Department of Otolaryngology Head and Neck Surgery. Production and hosting by Elsevier (Singapore) Pte Ltd. This is an open access article under the CC BY-NC-ND license (http://creativecommons.org/licenses/by-nc-nd/4.0/).

*Keywords:* Inner ear; Nanotechnology; Imaging; Gene delivery; Contrast agents

## Contents



☆ This study was supported by the National Natural Science Foundation of China (grant number: 81170914/H1304).

* Corresponding author. Department of Otolaryngology – Head and Neck Surgery, Changhai Hospital, Second Military Medical University, Changhai Road #168, Shanghai 200433, China.

*E-mail addresses:* zoujinghb@hotmail.com, Jing.Zou@uta.fi (J. Zou).

Peer review under responsibility of PLA General Hospital Department of Otolaryngology Head and Neck Surgery.

http://dx.doi.org/10.1016/j.joto.2016.11.002

1672-2930/Copyright © 2016, PLA General Hospital Department of Otolaryngology Head and Neck Surgery. Production and hosting by Elsevier (Singapore) Pte Ltd. This is an open access article under the CC BY-NC-ND license (http://creativecommons.org/licenses/by-nc-nd/4.0/).

## 1. Background

The inner ear is deeply buried within the temporal bone, which contains a dense bone lining, the entry points for the cochlear and vestibular nerves and the passageway for the facial nerve. The inner ear houses a membranous labyrinth that separates the spaces containing the endolymph and perilymph. Access to sensory elements in the inner ear is restricted by membranous partitions. Although hearing and balance problems are common, the diagnosis and treatment of inner ear diseases is hampered by the unique anatomy of the temporal bone and the limited access to the inner ear due to the relatively tight windows facing the middle ear and the blood-inner ear barriers, which allow homeostasis of the inner ear. Nanomedicine, including advanced drug delivery systems, new therapies, and *in vivo* imaging, is the future medicine that may overcome the shortcomings of the conventional medicine by delivering agents to specific cells, protecting the therapeutic contents, and controlling the cargo release (Pyykko, 2012; Senn, 2013). Potentional problems for nanomedicine related to toxicity and environmental impact of engineered nanomaterials (ENMs), which has drawn attention of researchers (Reuther, 2016). ENMs can potentially pass through these tight borders and enter the inner ear that might be applied in the clinics of Otology. A number of materials, for example genes and neurotrophins, among others, have been delivered to the inner ear, to facilitate the future treatment of inner ear disorders as well as improving imaging and diagnosis of inner ear conditions. Inner ear imaging is a very important issue in the research of nanomedicine of Otology, such as diagnosing hearing loss and vestibular malfunction, monitoring the behavior of ENMs within the inner ear and evaluating the outcomes of treatments. This review focuses on the access of ENMs to the inner ear, their passage of inner ear barriers and nanomedicine-augmented imaging of the inner ear.

## 2. The pathways and biological barriers of the inner ear regarding drug delivery

The biological barriers restricting access to the inner ear are the blood-perilymph barrier, blood-endolymph barrier, perilymph-endolymph barrier, and middle-inner ear barriers (the round window membrane and annular ligament of the oval window) (Zou et al., 2003, 2005a, 2012a; Counter et al., 1999, 2003; Zou et al., 2010a) (Fig. 1). The blood-perilymph barrier is mainly located in the vasculature region of the modiolus, where the transportation of substances from the blood into the perilymph in the scala vestibuli and scala tympani occurs (Zou et al., 2009a). The structures most likely responsible for this function are the cochlear glomeruli of Schwalbe, which are further divided into the upper glomeruli in the bony wall adjacent to the scala vestibuli and lower glomeruli in the osseous spiral lamina, which form vascular loops composed of anastomosed capillaries with a caliber of less than 10 microns (Franz et al., 1993; Penha et al., 1999). The modiolar walls of the first and second turns of the scala vestibuli and scala tympani are porous, forming a perilymphatic communication route to the perivascular and perineural spaces within the modiolus (Rask-Andersen et al., 2006). For example, gadolinium chelate (GdC) passes more readily to the scala tympani than to the scala vestibuli (Pyykko, 2012). Endolymph is isolated from the perilymph and blood by the tight junctions between the epithelial cells of Reissner's membrane that line the scala media (perilymph-endolymph barrier), those between the stria marginal cells (blood-endolymph barrier), and those in the reticular lamina, among others (Sakagami et al., 1984, 1991). The round window membrane is a sandwich-like structure that is composed of an outer squamous epithelial layer that faces the middle ear cavity, a medial connective tissue core, and an inner mesothelial layer that faces the scala tympani (Goycoolea, 2001; Goycoolea and Lundman, 1997). Transmission electron microscopy of rat round window membrane was shown in Fig. 2 (author's own data). The outer layer of the round window is composed of one or two layers of squat cuboidal cells that are

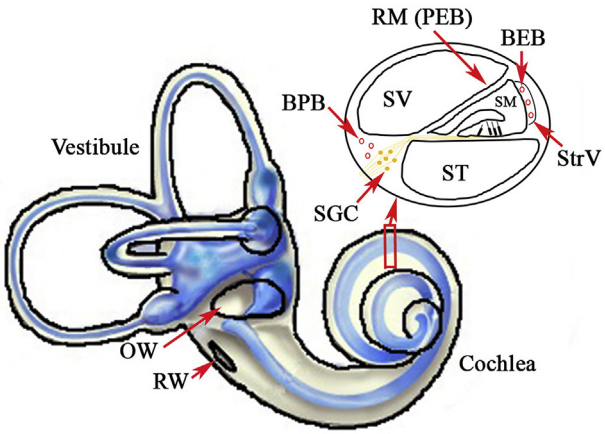


Fig. 1. Illustration showing the barriers within the inner ear. The middle-inner ear barriers consist of the oval window (OW) and the round window (RW). The blood-inner ear barriers consist of the blood-endolymph barrier (BEB) and the blood-perilymph barrier (BPB). Reissner's membrane (RM) forms the perilymph-endolymph barrier (PEB). SGC: spiral ganglion cell; SM: scala media; ST: scala tympani; StrV: stria vascularis; SV: scala vestibuli.

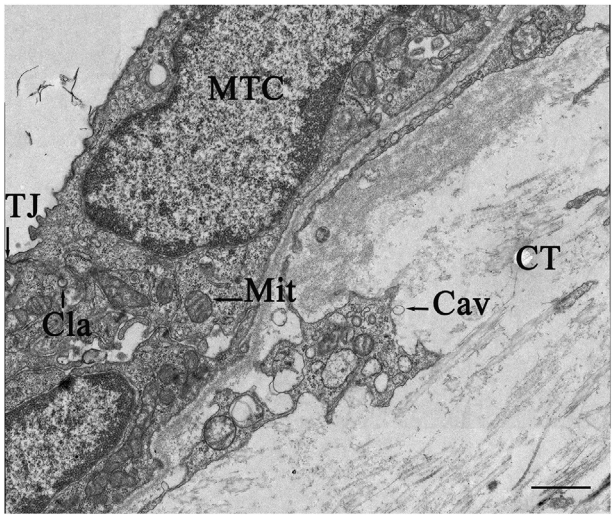


Fig. 2. Ultrastructure of the rat round window membrane. A rat round window membrane was en bloc contrasted using 1% $OsO_4$ (containing 2.22% $CaCl_2$) for 60 min, followed by staining with 2% uranyl acetate for 45 min at RT. The sample was then embedded in Epon. Thin sections were examined using a transmission electron microscope [Philips CM100 microscope equipped with a 1K digital camera system and Tietz software for capturing and processing (e.g., tiling) digital electron micrographs]. CAV: caveolae; Cla: clathrin; CT: connective tissue; Mit: mitochondria; MTC: mesothelial cells; TJ: tight junction. Scale bar = 847 nm.

continuous with the epithelium of the middle ear. Tight junctions are present near the surface of these cells (Schachern et al., 1982; Kawabata and Paparella, 1971). The oval window to which the ossicular chain is connected is a different structure, with the stapedial footplate occupying most of its area and which is linked to the bony lining of the oval window via the annular ligament. A histological study of rat inner ears demonstrated that the annular ligament of the stapediovestibular joint is a porous structure composed of fibrillin, a 36 kD microfibril-associated glycoprotein, and hyaluronic acid (Ohashi et al., 2008). The evidence that transport across the oval window can occur was obtained in guinea pigs as early as 1981 using horseradish peroxidase (HRP) as the tracer, although this finding was neglected due to the limitations of imaging techniques at the time, which did not allow real-time dynamic quantification of signals in the entire inner ear (Tanaka and Motomura, 1981). The delivered ENMs have to pass through these barriers before reaching the targets in the inner ear.

An ENM is defined as a material of 1−100 nm in at least one dimension, which can be a zero-dimensional (0-D), one-dimensional (1-D), two-dimensional (2-D), or three-dimensional (3-D) material (Whitesides, 2003). 0-D ENMs include nanoclustered materials and nanodispersions, i.e., materials in which the nanoparticles are isolated from one another. 1-D ENMs are nanofibrillar (nanorod) and nanotubular materials with a fiber (rod, tube) length of 100 nm to tens of microns. 2-D ENMs are films (coatings) of nanometer thicknesses. 3-D ENMs include powders and fibrous, multilayered and polycrystalline materials in which 0D, 1D and 2D structural elements are in close contact with one another and form interfaces (Fig. 3). ENMs can pass biological barriers through intracellular, paracellular, and transcellular pathways. Internalization of ENMs, which is affected by the size, shape, and surface charge of the particles, occurs by pinocytosis, micropinocytosis or phagocytosis. Generally, the smaller the size of an ENM, the more effective is its internalization (Murugan et al., 2015; Chithrani et al., 2006). The binding and activation of membrane receptors and the subsequent protein expression upon contact with an EMN strongly depend on the size of the nanoparticle, with 40- and 50-nm nanoparticles having the largest effect on signaling processes that are essential for basic cellular functions (Jiang et al., 2008). Spherical particles have a higher probability of internalization than rod-shaped nanoparticles (Chithrani et al., 2006). Taking quantum dots as an example, charged quantum dots have a higher internalization efficacy than do neutral dots, and anionic quantum dots have the highest uptake rate among all of the types of quantum dots (Liu et al., 2015).

To access defined compartments within the cochlea, ENMs must pass through either the middle-inner ear barriers or the blood-perilymph barrier, depending on the delivery approach (Zou et al., 2003, 2005a, 2010a, 2012a; Counter et al., 1999, 2003). Traditionally, oral administration and intravenous injection have been utilized in the delivery of drugs to treat inner ear diseases that take the pathway of blood-perilymph barrier (Zou et al., 2003). In 1991, Itoh and Sakata first reported performing an intratympanic dexamethasone injection as well as inner ear anesthesia using lidocaine for the treatment of patients with Meniere's disease or labyrinthine vertigo due to circulatory disturbances of the inner ear, for whom conservative treatments had failed (Itoh and Sakata, 1991). The efficient round and oval windows are involved in the intratympanic

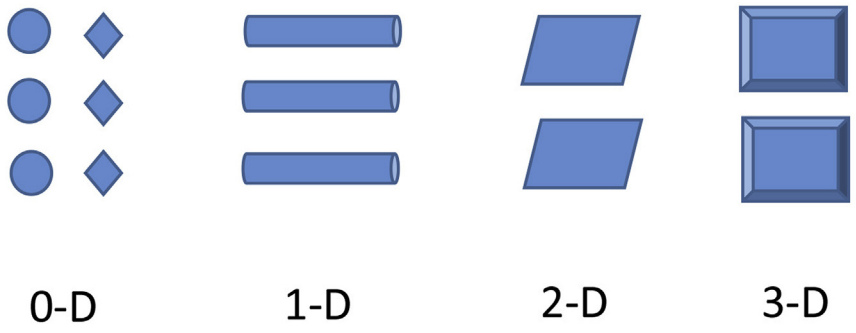


Fig. 3. Illustration showing the different dimensions of engineered nanomaterials.

administration (Zou et al., 2005a, 2010a, 2010b, 2011a, 2012a). Currently, intratympanic steroid injection is well accepted in the clinic as an alternative treatment for sudden sensorineural hearing loss (SNHL) and Meniere's disease even in non-specific formulations, in addition to other therapies. A multicenter study that compared the efficacy of intratympanic steroid injection with that of systemic steroid delivery as an initial treatment of SNHL complicated by diabetes demonstrated that the two methods were equally effective in inducing hearing gain and had similar recovery rates. However, an intratympanic injection was safer than the administration of systemic steroids (Han et al., 2009). In general, individuals were exposed to a significantly lower dose of agents upon intratympanic injection than upon systemic administration of agents even in non-specific formulations, which might be the reason for the different safety levels of the intratympanic injection and systemic administration of steroids (Zou et al., 2005a, 2010a, 2010b; Counter et al., 1999, 2003; Szebeni and Storm, 2015).

The intratympanic approach is important for nanomedical treatment because it reduces the potential for complement activation-related pseudoallergy and immunoreactions that can be induced by intravenously injected ENMs because topical delivery minimizes the interaction of the ENMs with the immune system (Szebeni and Storm, 2015; Shimizu et al., 2015; Banda et al., 2014). Regarding nanomedicine delivery, superparamagnetic iron oxide nanoparticles that are hierarchically coated with oleic acid and Pluronic®F127 copolymers (POA@SPIONs), superparamagnetic maghemite (g-$Fe_2O_3$) nanoparticles (NPs) generated using the ceric ammonium nitrate (CAN)-mediated oxidation of $Fe_3O_4$ (CAN-γ-$Fe_2O_3$ NPs), liposomal nanocarriers, lipid core nanocapsules (LNCs), and PEG-b-PCL polymersomes pass the middle-inner ear barriers to various extents (Zou et al., 2008, 2010c, 2010d, 2012b, 2015a, 2016a; Zhang et al., 2011a). The pathways through which ENMs enter the inner ear were displayed using *in vivo* MRI analysis, which showed that liposomal nanocarriers use the round window membrane as a major route and use the oval window as an additional route (Zou et al., 2014a). However, CAN-γ- $Fe_2O_3$ NPs use both the round and oval windows as the major pathways to enter the inner ear and penetrate the perilymph-endolymph barrier (Zou et al., 2016a). POA@SPIONs and liposomal nanocarriers did not penetrate the perilymph-endolymph barrier (Zou et al., 2010c, 2010d).

## 3. The beneficial applications and limitations of imaging techniques suitable for inner ear research

There are many choices of imaging techniques for the research in nanomedicine (Table 1). The different imaging techniques, such as magnetic resonance imaging (MRI), confocal microscopy, X-ray microtomography (μCT), optical projection tomography (OPT), and Cone-beam computed tomography (CBCT), will be introduced as followings in a priority order of relevance to nanomedicine-augmented imaging of the inner ear. Although CBCT has poor sensitivity in detecting ENMs, it is valuable in visualizing the locations of the electrodes of inserted cochlear implants and following ENM release from the future electrode equipped with regenerating system and following growth of auditory nerve fibers under neurotrophin stimulation towards the electrodes (Senn, 2013). Stimulated-emission-depletion (STED) microscopy and two-photon excitation (TPE)/selective plane illumination microscopy (SPIM), and coherent anti-Stokes Raman spectroscopic (CARS) microendoscopy will be discussed in the section of future perspectives for inner ear imaging using ENMs. Positron emission tomography (PET) will not be discussed due to the poor 3-dimensional resolution and non-applicability in the inner ear imaging.

Table 1
Imaging tools that have been applied in the research of nanomedicine.

| Imaging tools | Spatial resolution | Sensitivity | Applications |
|---|---|---|---|
| MRI | ≥50 μm | ++++ | *in vitro, in vivo* |
| confocal | ≥200 nm | +++++ | *in vitro, Ex vivo* |
| STED | ≥20 nm | +++++++ | *in vitro* |
| TPE | ≥200 nm | +++++ | *in vitro, Ex vivo* |
| SPIM | ≥320 nm | ++++++ | *in vitro, Ex vivo* |
| CARS | ≥200 nm | ++++++ | *in vitro, Ex vivo* |
| OPT | ≥2 μm | ++++ | *in vitro, Ex vivo* |
| μCT | ≥0.7 μm | ++ | *Ex vivo* |
| CBCT | ≥100 μm | + | *in vitro, in vivo* |
| PET | ≥125 μm | ++++++++ | *in vitro, in vivo* |

CARS: coherent anti-Stokes Raman spectroscopic microendoscopy; CBCT: cone-beam computed tomography; confocal: confocal microscopy; MRI: magnetic resonance imaging; OPT: optical projection stomography; PET: positron emission tomography; SPIM: selective plane illumination microscopy; STED: stimulated-emission-depletion microscopy; TPE: two-photon excitation; μCT: X-ray microtomography.

### 3.1. MRI

MRI depends on the magnetic properties of certain atomic nuclei and provides information on both the structures and functions of tissues without exposure to ionizing radiation. Due to the high spatial resolution and sensitivity of MRI, this technique has been broadly applied in the clinic and in nanomedicine. However, MRI was less useful than computed tomography (CT) in assessing patients with SNHL and vestibular disorders of the peripheral type, among others, during the 1980s, due to its poor resolution of bony structures (Valvassori, 1986). Most of the previously utilized imaging techniques focused on the bony fine structures of the inner ear and were unable to detect functional changes. Using MR spectrometry (MRS), metabolic changes can be detected with limited spectral resolution and low sensitivity. The application of isotopically labeled compounds (e.g., [1-$^{13}$C] glucose) enhanced the spectral resolution and sensitivity of MRS, although high levels of uncertainty and unreliability were reported (Shestov et al., 2007). Moreover, MRS can be applied to only relatively large homogenous tissues and cannot be used to visualize a heterogeneous area or finely structured organs, such as the inner ear. Separate demonstrations of the cochlear scalae in guinea pigs using high-resolution gadolinium chelate-enhanced MRI showed that it is possible to track functional alterations in the biological barriers of the inner ear

using this technique (Zou et al., 2003, 2005b, 2006, 2007, 2011b; Counter et al., 1999, 2003, 2000). Using the same technique, endolymphatic hydrops was detected in animal models and patients with Meniere's disease (Zou et al., 2000). Recently, calcium metabolic activity in the rat inner ear were followed using manganese-enhanced MRI, which proved that it is possible to monitor molecular activity in the inner ear *in vivo* (Zou and Pyykko, 2016).

ENMs that are functionalized with specific peptides or antibodies have been shown to be effective imaging contrast agents that allow MRI at a molecular level. Due to the contrast afforded by the use of certain ENMs, it was possible to follow the distribution of ENMs in the inner ear *in vivo* using MRI (Zou et al., 2010c, 2010d, 2012b, 2016a; Zhen et al., 2013). However, detecting ENMs in the inner ear using MRI is limited by the sensitivity of this method (Zou et al., 2016b) (Table 2).

### 3.2. Confocal microscopy

Confocal microscopy (or confocal laser scanning microscopy) is an optical imaging technique that increases the optical resolution and contrast of a micrograph through the application of a spatial pinhole placed at the confocal plane of the lens, which eliminates the out-of-focus light. This technique enables the reconstruction of three-dimensional structures from stacks of images collected at different depths (optical sectioning) within a thick object. Confocal microscopy has been extensively applied in biomedicine for *in vitro* studies. In the field of inner ear nanomedicine, confocal microscopy has been used to observe the cellular, extracellular, and subcellular localizations of ENMs in the inner ear in both cell culture and animal studies (Zou et al., 2008, 2014a; Zhang et al., 2011b, 2012; Pyykko et al., 2011; Surovtseva et al., 2012; Ahmad et al., 2015). Near-infrared fluorescence confocal laser endomicroscopy was reported to be capable of detecting αvβ3-integrin in colorectal tumors in a mouse model using an αvβ3-integrin optical probe (Schulz et al., 2015). A similar system could potentially be used in the future to conduct real-time molecular imaging within the ear.

### 3.3. μCT

μCT uses x-rays to create cross-sections of a physical object that can be used to recreate a virtual model (three-dimensional model) without destroying the original object, which requires a long imaging period and exposure to a high dose of radiation. μCT provided extremely high spatial-resolution (the pixel sizes of the cross-sections are in the micrometer range) inner ear images that revealed a membrane rupture within the cochlea. In temporal bones infused with 1 ml of 1% iodine, even the stria vascularis was distinguishable from the spiral ligament, and Reissner's membrane, among other structures, was visualized (Zou et al., 2015a) (Fig. 5). μCT was employed to microlocalize and quantitate Her2-targeted gold nanoparticles within tumor regions and the distribution of SPIONs in vascular tissue (Hainfeld et al., 2011; Tietze et al., 2011). Zou et al. (2015a, 2015b, 2015c) used μCT to visualize the distribution of transtympanically injected silver nanoparticles in the middle and inner ear of the rat and their transportation pathway following injection (Zou et al., 2015a). The detection sensitivity of μCT for ENMs varies broadly, depending on the chemical nature and size of the materials. The disadvantage of μCT for nanomedical research is that although it can demonstrate the functional properties of living organism, the high radiation dose that is required mandates sacrificing the experimental animals after *in vivo* experiments have been performed. Therefore, the application of μCT in studies of inner ear nanomedicine is limited, although the image resolution quality together with

Table 2
Visibility and passage of NPs through the round and oval windows in rats, as shown using MRI.

| Producers | Nanomaterials | Materials | Tag | Visibility | | Passage |
|---|---|---|---|---|---|---|
| | | | | *in vitro* | *in vivo* | |
| BIU | CAN−γ-$Fe_2O_3$ NPs | γ-$Fe_2O_3$, $Ce^{3/4+}$ | γ-$Fe_2O_3$ | +++++++ | +++++ | +++ |
| UHIB | LPN-Gd | Lipid, Gd-DOTA | Gd-DOTA | ++++ | +++ | +++ |
| ICCAS | $DF_1Gd_3$ | $C_{60}$ derivatives | Gd-DTPA | +++++ | ++++ | − |
| KTH | POA@SPIONs | $Fe_3O_4$, oleic acid, Pluronic® F127 copolymers | $Fe_3O_4$ | ++++++ | ++++ | +/− |
| UA | ACLNC | Lipid, Gd-DOTA | Gd-DOTA | + | − | Unknown |
| RWTH | MP-NG | PEG-DO3A, Gd-DOTA | Gd-DOTA | + | − | Unknown |
| USOU | Pn-NL-Gd | PLGA-PEG, Gd-DOTA | Gd-DOTA | ± | − | Unknown |
| TUT | ChNP-Gd | Chitosan, Gd-DOTA | Gd-DOTA | ± | − | Unknown |
| ABO | SiNP-Gd | Silica, Gd-DOTA | Gd-DOTA | − | − | Unknown |

Producers: ABO: Åbo Akademi University, Finland; BIU: Bar-Ilan University, Israel; EPFL: École polytechnique fédérale de Lausanne: Switzerland; ICCAS: Institute of Chemistry, Chinese Academy of Sciences, China; KTH: Royal Institute of Technology, Sweden; RWTH: Rheinisch-Westfälische Technische Hochschule Aachen, Germany; TUT: Tampere University of Technology, Finland; UA: University of Angers, France; UHIB: University of Helsinki, Institute of Biomedicine, Finland; USOU: University of Southampton, UK.

Nanomaterials: ACLNC: lipid core nanocapsules with gadolinium inside the core; CAN-γ-$Fe_2O_3$ NPs: superparamagnetic maghemite (g-$Fe_2O_3$) nanoparticles (NPs) generated using ceric ammonium nitrate (CAN)-mediated oxidation of $Fe_3O_4$ NPs; ChNP-Gd: gadolinium-containing chitosan nanoparticles; $DF_1Gd_3$: hydroxyl and amino-bearing $C_{60}$ derivatives ($C_{60}O_{\sim10}(NH_2)_{\sim7}(OH)_{\sim12}$) covalently binding with Gd-DTPA; LPN-Gd: gadolinium-containing liposome nanocarriers; MP-NG: gadolinium-containing PEG-DO3A nanogel; Pn-NL-Gd: gadolinium-containing PEG-b-PCL polymersomes; POA@SPIONs: superparamagnetic iron oxide nanoparticles hierarchically coated with oleic acid and Pluronic®F127 copolymers; SiNP-Gd: gadolinium-containing silica nanoparticles.

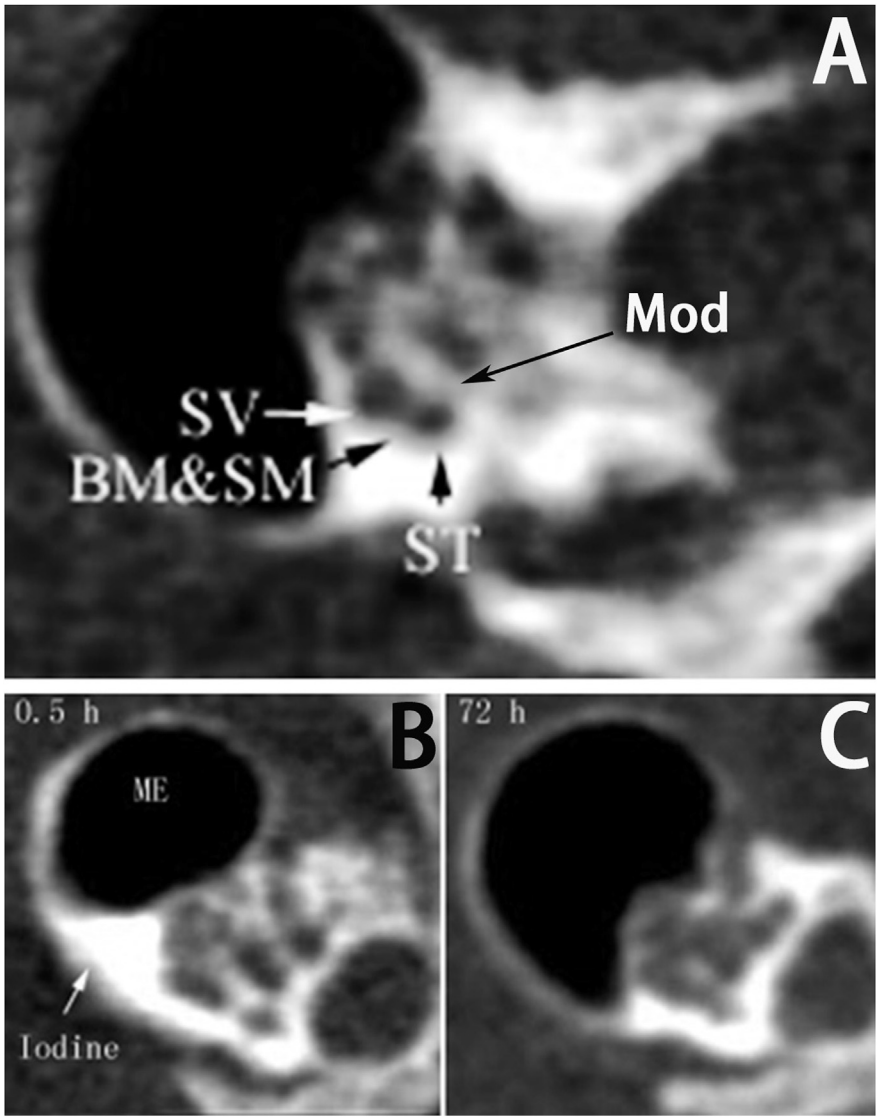


Fig. 4. CBCT images of the rat inner ear pre- and post-transtympanic injection of Iobitridol. The following imaging parameters were used in this study: number of frames, 900; tube voltage, 68 kV; tube current, 8 mA; exposure length per frame, 50 ms; and filtration, 0.5-mm copper + 2.5-mm aluminum. In rats that were not administered Iobitridol (A), the cochlear structures identified included the modiolus (Mod), scala tympani (ST), and scala vestibuli (SV). The basilar membrane (BM) and scala media (SM) were not distinguishable.

there being no need for physical sectioning provides at present the only option for obtaining a micrometer-scale image of the entire inner ear structure.

### 3.4. OPT

OPT is a non-destructive 3D imaging technique that was developed for the non-invasive analysis of small specimens in the mesoscopic range (Figueiras et al., 2014). OPT is a suitable technique for imaging hydrogel microstructures, which, using kurtosis and entropy, can be used to characterize hydrogels according to their optical properties (Figueiras et al., 2014). The mobility of FITC-dextran through a macroscopic hydrogel was analyzed using OPT, which showed that the velocities of the FITC-dextran particles were inversely proportional to the size of the dextrans, as expected (Soto et al., 2016). OPT was experimented to follow the diffusion of brain-derived neurotrophic factor (BDNF)-mimetic peptide-conjugated CAN−γ-$Fe_2O_3$ NPs within a BD™ PuraMatrix™ peptide hydrogel (BD Biosciences, Massachusetts, USA) and found that SPIONs were able to progress within the hydrogel (Fig. 6) (author's own data).

### 3.5. CBCT

CBCT is X-ray computed tomography in which the X-rays diverge to form a cone-beam and rotate around the target during image acquisition. The advantages that CBCT has over multi-detector CT (MDCT) are its rapid data acquisition rate, which is less than one minute versus several minutes for MDCT, the low-dose exposure of the subject, the small level of metallic artifact and the relatively low equipment purchase

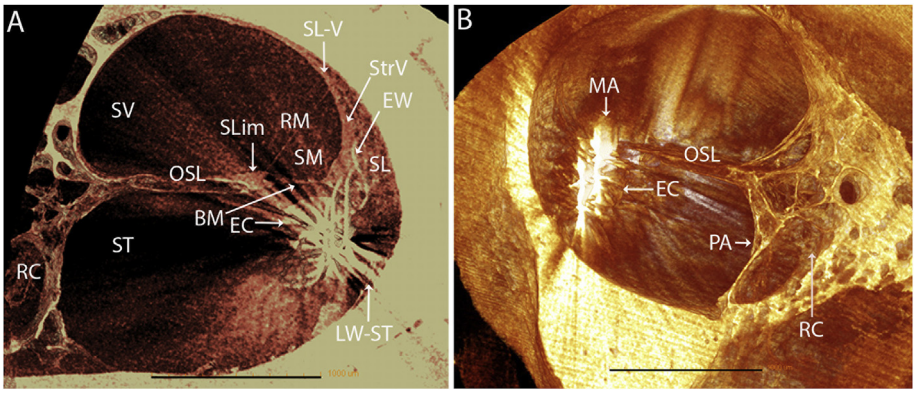


Fig. 5. Fine structure of an isolated human cochlea with an inserted cochlear implant electrode, as demonstrated using the 3-dimensional reconstruction of μCT images post-contrast treatment with iodine. In panel A, the scala tympani (ST), scala media (SM), and scala vestibuli (SV) are distinguishable, isolated by the osseous spiral lamina (OSL), basilar membrane (BM), and Reissner's membrane (RM). The specific tissues of the stria vascularis (StrV) and spiral ligament (SL), with fibrocyte type V cells in the lateral wall, are identifiable. At the beginning of the RM, the spiral limbus (Slim) is visible at the edge of the OSL. Rosenthal's canal (RC) and its nerve fibers are visible medial to the ST. The electrode contact (EC) and its metal wires (MW) are located below the BM. An overlapping image of the EW and SL was produced using the strong signal generated in the MW. In panel B, the details of the RC are demonstrated, and the medial wall of the ST showed a porous architecture (PA). Panels A and B are demonstrations of the same image captured at different orientations and with adjustments of contrast and brightness. LW-ST: lateral wall of the ST; MA: metal artifact. Scale bar = 1000 μm. Reprinted from Zou J et al. Hear. Res. 2015; 326:59–65.

price. CBCT is reportedly capable of demonstrating the fine structures of the middle and inner ear, as well as the pathological changes associated with otosclerosis and superior semicircular canal dehiscence (Zou et al., 2000, 2006; Zou and Pyykko, 2016). It is possible to distinguish even the cochlea scalae of rats using a commercial CBCT system, which showed that Iobitridol (a water-soluble, non-ionic, monomeric, low-osmolar, iodine-based contrast medium) did not pass the

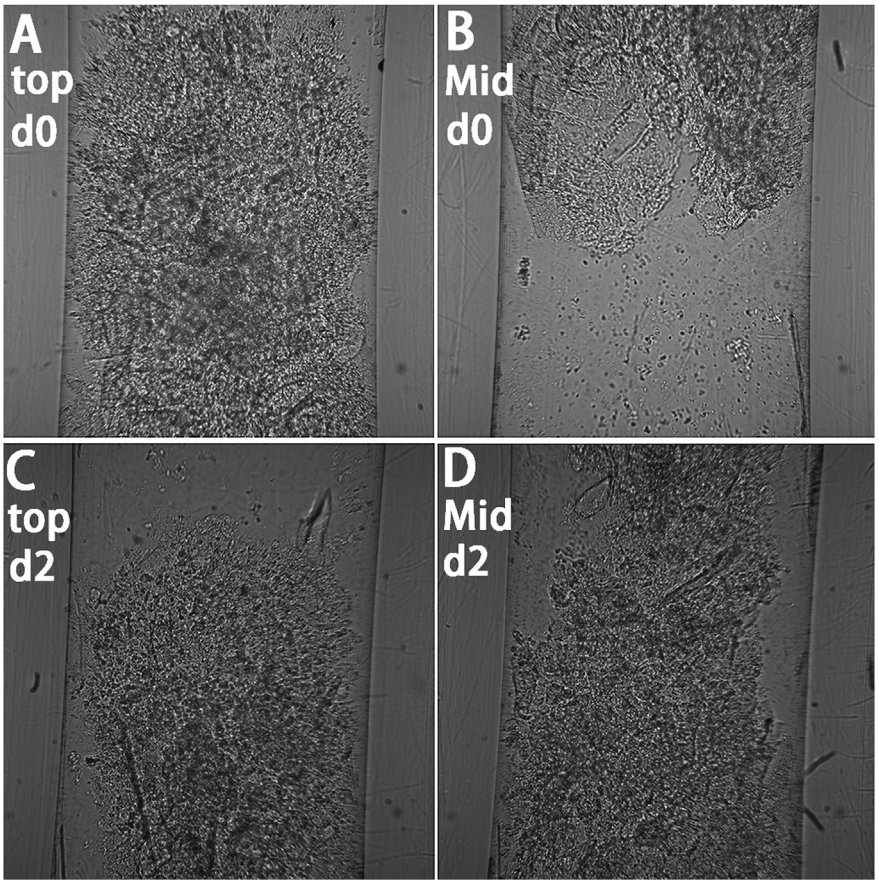


Fig. 6. Diffusion of SPIONs within a BD™ PuraMatrix™ peptide hydrogel, demonstrated using Optical projection tomography (OPT). BDNF-mimetic peptide-conjugated CAN–γ-$Fe_2O_3$ NPs at 0.2 mg/ml were added to the top of a tube containing the hydrogel, which was then imaged using OPT at d 0 and d 2. On d 0, the CAN–γ-$Fe_2O_3$ NPs remained in the top and middle portions of the tube (A, B). On d 2, the CAN–γ-$Fe_2O_3$ NPs had passed the middle portion of the tube (C, D).

middle-inner ear barriers or the blood-inner ear barriers (Fig. 4) (author's own data). The locations of the electrodes of inserted cochlear implants were accurately visualized using a novel high-resolution CBCT acquisition system that incorporates a pause during each exposure of multiple frames in combination with optimized filtration (Zou et al., 2015b, 2015c). Gold nanoparticles (AuNPs) have shown unique X-ray attenuation properties which, combined with their easy surface functionalization, makes them ideal candidates for the next generation of CT-imaging contrast agents. Moreover, glucosamine-functionalized gold nanoparticles have been developed for use as a CT contrast agent that combines spatial resolution with metabolic information (Silvestri et al., 2016). CT imaging will be promoted to the molecular level with the use of specific peptide or antibody-conjugated nanoparticles (Jiao et al., 2016). CBCT imaging can be improved to the same level using this nanotechnology.

## 4. Behavior of ENMs in inner ear applications

### 4.1. Imaging targetability

The nanomedical targets in the inner ear include molecules present in the normal architecture and those whose levels are elevated during pathological processes (Table 3). The therapeutic relevance of these molecules is uncertain. The principles for targeting architecture-specific molecules in the inner ear were tested, and a proof-of-concept for nanomedical targeting was obtained. Using TrkB-affinity peptides coupled to liposomal nanocarriers carrying the pGeneClipTM hMGFP plasmid encoding shRNA designed to transiently silence the inhibitor of differentiation and DNA binding-2 (Id2) and the EGFP reporter gene, targeting of the construct to spiral ganglion cells was observed in the adult rat cochlea using confocal microscopy (Zou et al., 2009b). Targeting of PEG-b-PCL polymersomes that were conjugated to the same peptides to spiral ganglion cells, Schwann cells, and nerve fibers was observed in organotypic explant cultures of mouse inner ears (Roy et al., 2010). Our pilot *in vivo* study using MRI for visualization also demonstrated the enrichment of the same type of liposomal nanocarriers in the cochlea (author's own data). In one study, a peptide called Tet1, which competes with tetanus toxin for GM1 binding, was conjugated to PEG-b-PCL polymersomes. The delivery of the Tet1-functionalized polymersomes via cochleostomy resulted in cochlear nerve targeting (Zhang et al., 2012). PEG6K-b-PCL polymersomes covalently labeled with peptides with an affinity for prestin, which were identified using phage display analysis, effectively targeted outer hair cells in a rat cochlear explant study, as shown using confocal microscopy (Surovtseva et al., 2012).

In addition to molecules present on the cellular surface, organelles are critical targets for gene delivery, and avoiding having the gene carriers trapped in endosomes is essential for their transfection. Ahmad et al. showed that three analogs of membrane-disrupting antimicrobial peptides (AMP), viz., LL-37, melittin, and bombolitin V, with glutamic acid substituted for all of the basic residues, are pH-sensitive and cause negligible membrane permeabilization and insignificant cytotoxicity at pH 7.4 (Ahmad et al., 2015). However, at pH 5.0, the prevailing targeting of endosomes, membrane binding and hemolysis of human erythrocytes became evident. The use of these AMPs resulted in expression levels comparable to those obtained using Lipofectamine 2000 (Ahmad et al., 2015).

Table 3
Molecular targets for imaging and drug delivery in the cochlea.

| Targets | Location | Expression | References |
|---|---|---|---|
| TrkB | SGC | Physiological | Ernfors et al. (1992) |
| GM1 | AN | Physiological | Santi et al. (1994) |
| Prestin | OHC | Physiological | Belyantseva et al. (2000) |
| TNFR | SCCO, SGC, SLF, SP | Pathological | Zou et al. (2005c) |
| VEGFR | MCST, OHC, SCCO, SGC, SLF | Pathological | Zou et al. (2005c) |

AN: auditory nerve; GM1: monosialotetrahexosyl ganglioside; MCST: mesothelial cell of scala tympani; OHC: outer hair cell; SCCO: supporting cells of Corti's organ; SGC: spiral ganglion cell; SLF: spiral ligament fibrocyte; SP: spiral prominence; TrkB: tropomyosin-related kinase B receptor.

### 4.2. Biological effects of the released cargo

The potential of liposomal nanoparticles and PEG-b-PCL polymersomes as therapeutic delivery systems into the cochlea via the round window membrane was evaluated using disulfiram, a neurotoxic agent, as a model payload. The delivery of disulfiram-loaded ENMs resulted in a significant decrease in the number of spiral ganglion cells, with an associated pronounced hearing loss, as assessed using auditory brainstem responses (Buckiova et al., 2012).

### 4.3. Gene expression mediated by ENMs

Nuclear entry is a critical step in gene delivery. To investigate the potential nuclear entry of hyperbranched polylysine nanoparticles (HPNPs) for gene delivery to cochlear targets, rat primary cochlear cells and cochlear explants obtained from newborn rats were treated with HPNPs at different concentrations (Zhang et al., 2011b). In the *in vivo* study using these nanoparticles, HPNPs were administered to the round window membranes of rats ad detected in different cell populations using confocal microscope after 24 h. Nuclear entry was detected in various cochlear cell types both *in vitro* and *in vivo* (Zhang et al., 2011b). In primary cochlear cell cultures, concentration-dependent internalization was observed. In cochlear organotypic cultures, abundant HPNPs were observed in the modiolus, including in the spiral ganglion, organ of Corti, and lateral wall tissues. In the *in vivo* study using these nanoparticles, a gradient distribution of HPNPs throughout different layers of the round window membrane was observed. HPNPs were also localized in cells within the tissues of the middle ear (Zhang et al., 2011b). Additionally, the effective internalization of HPNPs in the organ of Corti and spiral ganglion cells was observed. HPNPs yielded a higher transfection efficiency of primary cochlear cells than Lipofectamine™ (Zhang et al.,

2011b). These results suggest that HPNPs are potentially ideal carriers for gene delivery into the cochlea. Peptides that allow endosomal escape have been demonstrated to enhance gene expression. Three novel endosomolytic peptides have been discovered to be able to enhance gene expression mediated by liposomal ENMs (Ahmad et al., 2015).

Recently, Math1 gene therapy, in combination with the delivery of growth factors, was suggested to be the future treatment for deafness. Nuclear entry is necessary for the Math1 protein to exert transcription regulation through the enrichment and clustering of the MATH1-binding E-boxes of genes encoding nuclear receptors, such as Nr2f6, Hras1, and Hes5 (Krizhanovsky et al., 2006; Abdolazimi et al., 2016; Du et al., 2013). Zhang et al. constructed a pCDNA6.2/C-EmGFP-Math1 plasmid that expresses an EmGFP-Math1 fusion protein and followed the intracellular trafficking of Math1 protein under a confocal microscope. Zhang et al. detected a unique dynamic intracellular trafficking pattern of Math1 from the cytoplasm to the nucleus that was not observed in cells expressing exogenous brain-derived neurotrophic factor (BNDF) (Zhang et al., 2011c). However, the level of *in vivo* ENM-mediated gene expression in the inner ear was insufficient in our studies. Although Yoon et al. reported abundant *in vivo* EGFP expression in the modiolus of mice cochleae mediated by oligoarginine peptide (Arg8)-conjugated ENMs composed of poly(amino acid) (poly(2-hydroxyethyl L-aspartamide); PHEA) (Yoon et al., 2015), the ENMs in the published images were difficult to distinguish from the autofluorescent background.

### 4.4. Biocompatibility of ENMs in the inner ear

The safety of ENMs used for inner ear therapy must be proven in *in vitro* and *in vivo* studies before applying these materials to humans. Using confocal microscopy, HPNPs and LNCs have been detected in the cytoplasm of fibroblasts, with no sign of cytotoxic effects. After *in vivo* administration, these particles were visualized in cochlear cells, which did not cause any change in the hearing threshold or the loss of hair cells (Scheper et al., 2009). In the cited study, primary cochlear cells and mouse fibroblast cells treated with LNCs displayed toxicity only upon high dosage treatment. LNC administration to the middle ear did not cause hearing loss, nanoparticle exposure-related cell death or morphological changes in rat inner ear during 28 days of observation. Cochlear neural components, such as synaptophysin, ribbon synapses, and S-100, were not affected by the administration of LNCs. However, the expression level of neurofilament-200 was decreased in SGCs and in the cochlear nerve in the osseous spiral lamina canal following LNC delivery, a phenomenon that requires further investigation (Zhang et al., 2011d).

Using silver nanoparticles (AgNPs) as reference ENMs, Zou et al. detected significant changes in the permeability of biological barriers within the ear, including the middle ear mucosa, the skin of the external ear canal, and the inner ear at 5 h post-transtympanic injection of AgNPs at concentrations ranging from 20 to 4000 μg/ml. The alterations in permeability showed a dosage-response relationship and were reversible. Auditory brainstem response testing showed that administering 4000 μg/ml AgNPs induced hearing loss, with partial recovery occurring at 7 d post-treatment, whereas administering 20 μg/ml AgNPs caused reversible hearing loss (Zou et al., 2014b). The AgNPs caused significant hearing loss over a broad range of frequencies and induced the accumulation of glycosaminoglycan and hyaluronic acid in the basement membrane, and apoptosis in the AgNP-exposed organs was demonstrated by confocal microscopy (Feng et al., 2015). It was found that administering 0.4% AgNPs upregulated the expression of CD68, TLR4, MCP1, A20, and RNF11 in the strial basal cells, spiral ligament fibrocytes, and non-sensory supporting cells of the organ of Corti without affecting the levels of CD44, TLR2, MCP2, Rac1, myosin light chain, VCAM1, Erk1/2, JNK, p38, IL-1β, TNF-α, TNFR1, TNFR2, IL-10 or TGF-β. The results of this study suggested that AgNPs might confer macrophage-like functions to strial basal cells and spiral ligament fibrocytes and enhance the immune activities of the non-sensory supporting cells of the organ of Corti through upregulating the level of CD68, which might be involved in TLR4 activation. A20 and RNF11 play roles in maintaining cochlear homeostasis via negatively regulating the expression of inflammatory cytokines (Feng et al., 2015).

## 5. Future perspectives for inner ear imaging using ENMs

### 5.1. Advanced imaging techniques

I. Stimulated-emission-depletion (STED) microscopy and two-photon excitation (TPE)/selective plane illumination microscopy (SPIM)

Fluorescence microscopy is the imaging method that is most widely used in biology. However, the resolution power of far-field light microscopy is constrained by the diffraction limit of light, as explained by Ernst Abbe more than a century ago (Abbé, 1873). In 1994, Stefan Hell described a new type of scanning fluorescence microscope that was capable of resolving 35 nm in the far field by circumventing the optical diffraction limit, which is the STED microscope (Hell and Wichmann, 1994; Klar and Hell, 1999), a development for which he won the Nobel Prize in Chemistry in 2014. A STED microscope employs two overlapping synchronized laser beams that arrive at the sample position consecutively and of which the first one (excitation laser) excites and the second one (depletion or STED laser) de-excites (or depletes the excitation within) the sample. STED microscopy is a practical extension of confocal microscopy. In the region that both laser beams strike, stimulated emission occurs, and in the focal region that only the first excitation beam strikes, spontaneous emission (i.e., fluorescence) is observed. To apply this concept to microscopy, a phase mask must be placed in the path of the depletion laser, which creates a doughnut-shaped pattern. Pulsed lasers have been widely used in STED microscopy because they allow the precise control of the excitation and depletion cycles and the use of relatively a low power to

induce depletion. However, due to recent advances, effective STED systems with continuous wave (CW) lasers have been developed, which greatly simplify the implementation of this instrument by eliminating the synchronization units required for pulsed systems (Willig et al., 2007; Moneron et al., 2010; Vicidomini et al., 2011; Moffitt et al., 2011). Moreover, replacing mode-locked pulsed lasers with simple CW lasers reduces the cost of a STED optical system. The disadvantage of using CW lasers in a STED microscope is that a higher power output is needed and the continuous illumination of the sample using a CW laser increases the extent of photobleaching compared with that produced using pulsed lasers (Farahani et al., 2010).

TPE microscopy is an alternative to confocal microscopy that has advantages for three-dimensional and deep-tissue imaging. TPE arises from the simultaneous absorption of two photons in a single event (Goppert-Mayer, 1931; Kaiser, 1961). Each photon carries approximately half the energy necessary to excite a molecule. In contrast to the case for confocal microscopy, there is no absorption or fluorescence (and thus no photobleaching or phototoxicity) above and below the plane of focus in TPE microscopy. Longer wavelengths must be employed to increase the penetration depth in TPE microscopy, which has the drawback of reducing the spatial resolution. In addition, the exposure to high-power laser pulses over a long period may induce the detrimental effects of light, such as heating, photobleaching and photodamage (Huisken and Stainier, 2009). SPIM also allows optical sectioning by selectively exciting the target molecules through illuminating the sample from the side in a well-defined volume around the focal plane of the detection optics (Huisken and Stainier, 2009; Huisken et al., 2004). SPIM has advantages over TPE microscopy, such as high depth penetration, low-level photobleaching and high acquisition speeds, the latter of which is critical in extended time-lapse experiments. High-resolution three-dimensional (3D) live imaging of multicellular specimens was recently achieved using SPIM with real-time light-sheet optimization by tiling the excitation light sheet (Fu et al., 2016; Gao, 2015).

Moneron and Hell developed a TPE-STED microscope that uses a short-pulse laser for TPE and a CW laser source for resolution enhancement (STED), which achieves a resolution of <50 nm for fluorescent nanoparticles, which is a 5.4-fold improvement over the diffraction barrier (Moneron and Hell, 2009). However, none of these systems has been applied in inner ear research.

II. Coherent anti-Stokes Raman spectroscopic microendoscopy

Coherent anti-Stokes Raman spectroscopic (CARS) microendoscopy is a technique that is based on Raman scattering, a process in which incident photons scatter inelastically upon interacting with matter, which was discovered by Raman, who received the Nobel Prize in Physics in 1930 (Raman, 1922). CARS occurs when a target molecule is simultaneously irradiated by two laser beams operating at different frequencies, a pump beam $\omega_P$ and a Stokes beam $\omega_S$. When the difference between the higher (pump beam) frequency and the lower (Stokes beam) frequency equals the vibrational frequency of the targeted bond of a molecule, a CARS signal is generated (Pezacki et al., 2011; Folick et al., 2011). It was recently reported that a cholesteatoma in the mastoid and tympanic membrane was detected *in vitro* using CARS microscopy (Zou et al., 2016c). Some groups have reported the development of a CARS microendoscope although such a system requires further improvement before it is practical (Brustlein et al., 2011; Satira, 2013).

### 5.2. Improvements in imaging agents

Imaging agents must meet several requirements to be effective in visualizing the inner ear. First, the imaging agents must effectively generate signals in a defined imaging system. SPIONs have been proven highly effective MRI contrast agents (Zou et al., 2010c, 2016a). Gold nanoparticles (AuNPs) have recently been shown to be effective CT contrast agents that allowed tracking the recruitment of monocyte in atherosclerosis (Chhour et al., 2016). Gadolinium-fullerene (C60) derivatives (DF1Gd3) have been shown to be effective MRI and fluorescence imaging contrast agents (Zhen et al., 2013). Second, the imaging agents should be able to enter the inner ear by passing through its biological barriers. Neither DF1Gd3 nor POA@SPIONs passed through the middle-inner ear barriers and thus are unsuitable for inner ear imaging (Zou et al., 2010c; Zhen et al., 2013). CAN-γ- $Fe_2O_3$ NPs, liposomal ENMs, PEG-b-PCL polymersomes, LNCs, and HAuNPs are good candidate ENMs for inner ear imaging because they can enter the inner ear from the middle ear (Zou et al., 2008, 2010d, 2011a, 2012b, 2016a). Third, the imaging agents should accumulate specifically in the target cells following their delivery. In addition to the molecules expressed in an unstimulated condition that have been used in previous proof-of-concept studies (Surovtseva et al., 2012; Zhang et al., 2012; Zou et al., 2009b; Roy et al., 2010), pathological markers, such as tumor necrosis factor receptors and vascular endothelial growth factor receptors, as well as mitochondrial markers, should be included in future studies.

To conclude, there are several challenges to inner ear drug delivery and imaging due to the existence of tight biological barriers to the inner ear and the dense bone surrounding it. The oval window was recently discovered to be an extremely effective pathway through which agents could access the inner ear. ENMs are both effective carriers for drug delivery and novel contrast agents for molecular imaging. Among the various imaging techniques currently available, MRI is the most effective and feasible technique for both experimental and clinical inner ear imaging. μCT is useful for experimental inner ear imaging because its implementation does not require specimen processing. Confocal microscopy is the imaging method most commonly employed for inner ear histology, although STEM has a significantly higher degree of spatial resolution. CARS microendoscopy is an imaging technique that can be employed in the future for inner ear imaging at the

molecular level, with or without the use of ENM contrast agents (Pope et al., 2014).

## Acknowledgements

We thank Dr. Hao Feng for preparing the samples for OPT imaging, Dr. Edite Figueiras for performing OPT imaging, and Prof. Jean-Paul (Moshe) Lellouche and Dr. Stella Ostrovsky for preparing the BDNF-mimetic peptide-conjugated CAN–γ-$Fe_2O_3$ NPs. We thank Dr. Markus Hannula for assistance with CBCT imaging.

## References

Abbé, E., 1873. Beitrage zur Theorie des Mikroskops und der mikroskopischen Wahrnehmung. Arch. Mikrosk. Anat. 9, 413–420.

Abdolazimi, Y., Stojanova, Z., Segil, N., 2016. Selection of cell fate in the organ of Corti involves the integration of Hes/Hey signaling at the Atoh1 promoter. Development 143 (5), 841–850.

Ahmad, A., Ranjan, S., Zhang, W., Zou, J., Pyykko, I., Kinnunen, P.K., 2015. Novel endosomolytic peptides for enhancing gene delivery in nanoparticles. Biochim. Biophys. Acta 1848 (2), 544–553.

Banda, N.K., Mehta, G., Chao, Y., Wang, G., Inturi, S., Fossati-Jimack, L., et al., 2014. Mechanisms of complement activation by dextran-coated superparamagnetic iron oxide (SPIO) nanoworms in mouse versus human serum. Part Fibre Toxicol. 11, 64.

Belyantseva, I.A., Adler, H.J., Curi, R., Frolenkov, G.I., Kachar, B., 2000. Expression and localization of prestin and the sugar transporter GLUT-5 during development of electromotility in cochlear outer hair cells. J. Neurosci. 20 (24). RC116.

Brustlein, S., Berto, P., Hostein, R., Ferrand, P., Billaudeau, C., Marguet, D., et al., 2011. Double-clad hollow core photonic crystal fiber for coherent Raman endoscope. Opt. Express 19 (13), 12562–12568.

Buckiova, D., Ranjan, S., Newman, T.A., Johnston, A.H., Sood, R., Kinnunen, P.K., et al., 2012. Minimally invasive drug delivery to the cochlea through application of nanoparticles to the round window membrane. Nanomedicine (Lond) 7 (9), 1339–1354.

Chhour, P., Naha, P.C., O'Neill, S.M., Litt, H.I., Reilly, M.P., Ferrari, V.A., et al., 2016. Labeling monocytes with gold nanoparticles to track their recruitment in atherosclerosis with computed tomography. Biomaterials 87, 93–103.

Chithrani, B.D., Ghazani, A.A., Chan, W.C., 2006. Determining the size and shape dependence of gold nanoparticle uptake into mammalian cells. Nano Lett. 6 (4), 662–668.

Counter, S.A., Bjelke, B., Klason, T., Chen, Z., Borg, E., 1999. Magnetic resonance imaging of the cochlea, spiral ganglia and eighth nerve of the Guinea pig. Neuroreport 10 (3), 473–479.

Counter, S.A., Bjelke, B., Borg, E., Klason, T., Chen, Z., Duan, M.L., 2000. Magnetic resonance imaging of the membranous labyrinth during in vivo gadolinium (Gd-DTPA-BMA) uptake in the normal and lesioned cochlea. Neuroreport 11 (18), 3979–3983.

Counter, S.A., Zou, J., Bjelke, B., Klason, T., 2003. 3D MRI of the in vivo vestibulo-cochlea labyrinth during Gd-DTPA-BMA uptake. Neuroreport 14 (13), 1707–1712.

Du, X., Li, W., Gao, X., West, M.B., Saltzman, W.M., Cheng, C.J., et al., 2013. Regeneration of mammalian cochlear and vestibular hair cells through Hes1/Hes5 modulation with siRNA. Hear Res. 304, 91–110.

Ernfors, P., Merlio, J.P., Persson, H., 1992. Cells expressing mRNA for neurotrophins and their receptors during embryonic rat development. Eur. J. Neurosci. 4 (11), 1140–1158.

Farahani, J.N., Schibler, M.J., Bentolila, L.A., 2010. Stimulated emission depletion (STED) microscopy: from theory to practice. Microsc. Sci. Technol. Appl. Educ. 4 (2), 1539–1547.

Feng, H., Pyykko, I., Zou, J., 2015. Hyaluronan up-regulation is linked to renal dysfunction and hearing loss induced by silver nanoparticles. Eur. Arch. Otorhinolaryngol. 272 (10), 2629–2642.

Figueiras, E., Soto, A.M., Jesus, D., Lehti, M., Koivisto, J., Parraga, J.E., et al., 2014. Optical projection tomography as a tool for 3D imaging of hydrogels. Biomed. Opt. Express 5 (10), 3443–3449.

Folick, A., Min, W., Wang, M.C., 2011. Label-free imaging of lipid dynamics using Coherent Anti-stokes Raman Scattering (CARS) and Stimulated Raman Scattering (SRS) microscopy. Curr. Opin. Genet. Dev. 21 (5), 585–590.

Franz, P., Aharinejad, S., Bock, P., Firbas, W., 1993. The cochlear glomeruli in the modiolus of the Guinea pig. Eur. Arch. Otorhinolaryngol. 250 (1), 44–50.

Fu, Q., Martin, B.L., Matus, D.Q., Gao, L., 2016. Imaging multicellular specimens with real-time optimized tiling light-sheet selective plane illumination microscopy. Nat. Commun. 7, 11088.

Gao, L., 2015. Extend the field of view of selective plan illumination microscopy by tiling the excitation light sheet. Opt. Express 23 (5), 6102–6111.

Goppert-Mayer, M., 1931. Über Elementarakte mit zwei Quantensprüngen. Ann. Phys. 401 (3), 273–294.

Goycoolea, M.V., 2001. Clinical aspects of round window membrane permeability under normal and pathological conditions. Acta Otolaryngol. 121 (4), 437–447.

Goycoolea, M.V., Lundman, L., 1997. Round window membrane. Structure function and permeability: a review. Microsc. Res. Tech. 36 (3), 201–211.

Hainfeld, J.F., O'Connor, M.J., Dilmanian, F.A., Slatkin, D.N., Adams, D.J., Smilowitz, H.M., 2011. Micro-CT enables microlocalisation and quantification of Her2-targeted gold nanoparticles within tumour regions. Br. J. Radiol. 84 (1002), 526–533.

Han, C.S., Park, J.R., Boo, S.H., Jo, J.M., Park, K.W., Lee, W.Y., et al., 2009. Clinical efficacy of initial intratympanic steroid treatment on sudden sensorineural hearing loss with diabetes. Otolaryngol. Head Neck Surg. 141 (5), 572–578.

Hell, S.W., Wichmann, J., 1994. Breaking the diffraction resolution limit by stimulated emission: stimulated-emission-depletion fluorescence microscopy. Opt. Lett. 19 (11), 780–782.

Huisken, J., Stainier, D.Y., 2009. Selective plane illumination microscopy techniques in developmental biology. Development 136 (12), 1963–1975.

Huisken, J., Swoger, J., Del Bene, F., Wittbrodt, J., Stelzer, E.H., 2004. Optical sectioning deep inside live embryos by selective plane illumination microscopy. Science 305 (5686), 1007–1009.

Itoh, A., Sakata, E., 1991. Treatment of vestibular disorders. Acta Otolaryngol. Suppl. 481, 617–623.

Jiang, W., Kim, B.Y., Rutka, J.T., Chan, W.C., 2008. Nanoparticle-mediated cellular response is size-dependent. Nat. Nanotechnol. 3 (3), 145–150.

Jiao, P., Otto, M., Geng, Q., Li, C., Li, F., Butch, E.R., et al., 2016. Enhancing both CT imaging and natural killer cell-mediated cancer cell killing by a GD2-targeting nanoconstruct. J. Mater. Chem. B Mater. Biol. Med. 4 (3), 513–520.

Kaiser, W.G.C., 1961. Two-photon excitation in CaF2:Eu2+. Phys. Rev. Lett. 7, 229–231.

Kawabata, I., Paparella, M.M., 1971. Fine structure of the round window membrane. Ann. Otol. Rhinol. Laryngol. 80 (1), 13–26.

Klar, T.A., Hell, S.W., 1999. Subdiffraction resolution in far-field fluorescence microscopy. Opt. Lett. 24 (14), 954–956.

Krizhanovsky, V., Soreq, L., Kliminski, V., Ben-Arie, N., 2006. Math1 target genes are enriched with evolutionarily conserved clustered E-box binding sites. J. Mol. Neurosci. 28 (2), 211–229.

Liu, Q., Li, H., Xia, Q., Liu, Y., Xiao, K., 2015. Role of surface charge in determining the biological effects of CdSe/ZnS quantum dots. Int. J. Nanomedicine 10, 7073–7088.

Moffitt, J.R., Osseforth, C., Michaelis, J., 2011. Time-gating improves the spatial resolution of STED microscopy. Opt. Express 19 (5), 4242–4254.

Moneron, G., Hell, S.W., 2009. Two-photon excitation STED microscopy. Opt. Express 17 (17), 14567–14573.

Moneron, G., Medda, R., Hein, B., Giske, A., Westphal, V., Hell, S.W., 2010. Fast STED microscopy with continuous wave fiber lasers. Opt. Express 18 (2), 1302–1309.

Murugan, K., Choonara, Y.E., Kumar, P., Bijukumar, D., du Toit, L.C., Pillay, V., 2015. Parameters and characteristics governing cellular internalization and trans-barrier trafficking of nanostructures. Int. J. Nanomedicine 10, 2191–2206.

Ohashi, M., Ide, S., Sawaguchi, A., Suganuma, T., Kimitsuki, T., Komune, S., 2008. Histochemical localization of the extracellular matrix components in the annular ligament of rat stapediovestibular joint with special reference to fibrillin, 36-kDa microfibril-associated glycoprotein (MAGP-36), and hyaluronic acid. Med. Mol. Morphol. 41 (1), 28–33.

Penha, R., O'Neill, M.A., Goyri O'Neill, J., Esperanca Pina, J.A., 1999. Ultrastructural aspects of the microvasculature of the cochlea: the internal spiral network. Otolaryngol. Head Neck Surg. 120 (5), 725–729.

Pezacki, J.P., Blake, J.A., Danielson, D.C., Kennedy, D.C., Lyn, R.K., Singaravelu, R., 2011. Chemical contrast for imaging living systems: molecular vibrations drive CARS microscopy. Nat. Chem. Biol. 7 (3), 137–145.

Pope, I., Payne, L., Zoriniants, G., Thomas, E., Williams, O., Watson, P., et al., 2014. Coherent anti-stokes Raman scattering microscopy of single nanodiamonds. Nat. Nanotechnol. 9 (11), 940–946.

Pyykko, I., 2012. NANOEAR-3g-Nanotechnology Based Targeted Drug Delivery Using the Inner Ear as a Model Target Organ: CORDIS. Available from: http://cordis.europa.eu/project/rcn/81536_en.html.

Pyykko, I., Zou, J., Zhang, W., Zhang, Y., 2011. Nanoparticle-based delivery for the treatment of inner ear disorders. Curr. Opin. Otolaryngol. Head Neck Surg. 19 (5), 388–396.

Raman, C.V., 1922. Molecular Diffraction of Light. February 11. University of Calcutta, Calcutta, pp. 1–103.

Rask-Andersen, H., Schrott-Fischer, A., Pfaller, K., Glueckert, R., 2006. Perilymph/modiolar communication routes in the human cochlea. Ear Hear 27 (5), 457–465.

Reuther, R., 2016. NanoValid-developing Reference Methods for Nanomaterials: European Union. Available from: http://www.nanovalid.eu/.

Roy, S., Johnston, A.H., Newman, T.A., Glueckert, R., Dudas, J., Bitsche, M., et al., 2010. Cell-specific targeting in the mouse inner ear using nanoparticles conjugated with a neurotrophin-derived peptide ligand: potential tool for drug delivery. Int. J. Pharm. 390 (2), 214–224.

Sakagami, M., Sano, M., Matsunaga, T., 1984. Ultrastructural study of the effect of acute hypertension on the stria vascularis and spiral ligament. Acta Otolaryngol. 97 (1–2), 53–61.

Sakagami, M., Fukazawa, K., Kitamura, K., Doi, K., Mori, N., Matsunaga, T., 1991. Transport of HRP through Reissner's membrane in experimental endolymphatic hydrops. Acta Otolaryngol. 111 (5), 872–878.

Santi, P.A., Mancini, P., Barnes, C., 1994. Identification and localization of the GM1 ganglioside in the cochlea using thin-layer chromatography and cholera toxin. J. Histochem. Cytochem. 42 (6), 705–716.

Satira, Z.A., 2013. Theoretical Investigation of Material Properties Affecting Coherent Anti-stokes Raman Scattering Microendoscopy. Rice University, Ann Arbor, Houston, Texas.

Schachern, P.A., Paparella, M.M., Duvall 3rd, A.J., 1982. The normal chinchilla round window membrane. Arch. Otolaryngol. 108 (9), 550–554.

Scheper, V., Wolf, M., Scholl, M., Kadlecova, Z., Perrier, T., Klok, H.A., et al., 2009. Potential novel drug carriers for inner ear treatment: hyperbranched polylysine and lipid nanocapsules. Nanomedicine (Lond) 4 (6), 623–635.

Schulz, P., Dierkes, C., Wiedenmann, B., Grotzinger, C., 2015. Near-infrared confocal laser endomicroscopy detects colorectal cancer via an integrin alphavbeta 3 optical probe. Mol. Imaging Biol. 17 (4), 450–460.

Senn, P., 2013. NANOCI-Nanotechnology Based Cochlear Implant: SCIPROM. Available from: http://www.nanoci.org/.

Shestov, A.A., Valette, J., Ugurbil, K., Henry, P.G., 2007. On the reliability of (13)C metabolic modeling with two-compartment neuronal-glial models. J. Neurosci. Res. 85 (15), 3294–3303.

Shimizu, T., Mima, Y., Hashimoto, Y., Ukawa, M., Ando, H., Kiwada, H., et al., 2015. Anti-PEG IgM and complement system are required for the association of second doses of PEGylated liposomes with splenic marginal zone B cells. Immunobiology 220 (10), 1151–1160.

Silvestri, A., Zambelli, V., Ferretti, A.M., Salerno, D., Bellani, G., Polito, L., 2016. Design of functionalized gold nanoparticle probes for computed tomography imaging. Contrast Media Mol. Imaging 11 (5), 405–414.

Soto, A.M., Koivisto, J.T., Parraga, J.E., Silva-Correia, J., Oliveira, J.M., Reis, R.L., et al., 2016. Optical projection tomography technique for image texture and mass transport studies in hydrogels based on gellan gum. Langmuir 32 (20), 5173–5182.

Surovtseva, E.V., Johnston, A.H., Zhang, W., Zhang, Y., Kim, A., Murakoshi, M., et al., 2012. Prestin binding peptides as ligands for targeted polymersome mediated drug delivery to outer hair cells in the inner ear. Int. J. Pharm. 424 (1–2), 121–127.

Szebeni, J., Storm, G., 2015. Complement activation as a bioequivalence issue relevant to the development of generic liposomes and other nanoparticulate drugs. Biochem. Biophys. Res. Commun. 468 (3), 490–497.

Tanaka, K., Motomura, S., 1981. Permeability of the labyrinthine windows in Guinea pigs. Arch. Otorhinolaryngol. 233 (1), 67–73.

Tietze, R., Rahn, H., Lyer, S., Schreiber, E., Mann, J., Odenbach, S., et al., 2011. Visualization of superparamagnetic nanoparticles in vascular tissue using XmuCT and histology. Histochem. Cell Biol. 135 (2), 153–158.

Valvassori, G.E., 1986. Applications of magnetic resonance imaging in otology. Am. J. Otol. 7 (4), 262–266.

Vicidomini, G., Moneron, G., Han, K.Y., Westphal, V., Ta, H., Reuss, M., et al., 2011. Sharper low-power STED nanoscopy by time gating. Nat. Methods 8 (7), 571–573.

Whitesides, G.M., 2003. The 'right' size in nanobiotechnology. Nat. Biotechnol. 21 (10), 1161–1165.

Willig, K.I., Harke, B., Medda, R., Hell, S.W., 2007. STED microscopy with continuous wave beams. Nat. Methods 4 (11), 915–918.

Yoon, J.Y., Yang, K.J., Kim da, E., Lee, K.Y., Park, S.N., Kim, D.K., et al., 2015. Intratympanic delivery of oligoarginine-conjugated nanoparticles as a gene (or drug) carrier to the inner ear. Biomaterials 73, 243–253.

Zhang, Y., Zhang, W., Johnston, A.H., Newman, T.A., Pyykk, I., Zou, J., 2011. Comparison of the distribution pattern of PEG-b-PCL polymersomes delivered into the rat inner ear via different methods. Acta Otolaryngol. 131 (12), 1249–1256.

Zhang, W., Zhang, Y., Lobler, M., Schmitz, K.P., Ahmad, A., Pyykko, I., et al., 2011. Nuclear entry of hyperbranched polylysine nanoparticles into cochlear cells. Int. J. Nanomedicine 6, 535–546.

Zhang, W., Zhang, Y., Sood, R., Ranjan, S., Surovtseva, E., Ahmad, A., et al., 2011. Visualization of intracellular trafficking of Math1 protein in different cell types with a newly-constructed nonviral gene delivery plasmid. J. Gene Med. 13 (2), 134–144.

Zhang, Y., Zhang, W., Lobler, M., Schmitz, K.P., Saulnier, P., Perrier, T., et al., 2011. Inner ear biocompatibility of lipid nanocapsules after round window membrane application. Int. J. Pharm. 404 (1–2), 211–219.

Zhang, Y., Zhang, W., Johnston, A.H., Newman, T.A., Pyykko, I., Zou, J., 2012. Targeted delivery of Tet1 peptide functionalized polymersomes to the rat cochlear nerve. Int. J. Nanomedicine 7, 1015–1022.

Zhen, M., Zheng, J., Wang, Y., Shu, C., Gao, F., Zou, J., et al., 2013. Multifunctional nanoprobe for MRI/optical dual-modality imaging and radical scavenging. Chemistry 19 (43), 14675–14681.

Zou, J., Pyykko, I., 2016. Calcium metabolism profile in rat inner ear indicated by MRI after tympanic medial wall administration of manganese chloride. Ann. Otol. Rhinol. Laryngol. 125 (1), 53–62.

Zou, J., Pyykko, I., Bjelke, B., Bretlau, P., Tayamaga, T., 2000. Endolympahtic Hydrops Is Caused by Increased Porosity of Stria Vascularis? Barany Society Meeting, Uppsala, Sweden.

Zou, J., Pyykko, I., Counter, S.A., Klason, T., Bretlau, P., Bjelke, B., 2003. In vivo observation of dynamic perilymph formation using 4.7 T MRI with gadolinium as a tracer. Acta Otolaryngol. 123 (8), 910–915.

Zou, J., Pyykko, I., Bjelke, B., Dastidar, P., Toppila, E., 2005. Communication between the perilymphatic scalae and spiral ligament visualized by in vivo MRI. Audiol. Neurootol. 10 (3), 145–152.

Zou, J., Ilmari, P., Borje, B., Counter, S.A, 2005. MRI evidence of exogenous vascular endothelial growth factor-enhanced transport across inner ear barriers in Guinea pigs. Zhonghua Er Bi Yan Hou Tou Jing Wai Ke Za Zhi 40 (4), 266–270.

Zou, J., Pyykko, I., Sutinen, P., Toppila, E., 2005. Vibration induced hearing loss in Guinea pig cochlea: expression of TNF-alpha and VEGF. Hear Res. 202 (1–2), 13–20.

Zou, J., Pyykko, I., Sutinen, P., Toppila, E., 2006. MRI presentation of the blood-labyrinth barrier change after cochlea vibration trauma. Chin. J. Otol. 4 (1), 61–64.

Zou, J., Pyykko, I., Bjelke, B., Toppila, E., 2007. In vivo MRI visualization of endolymphatic hydrops induced by keyhole limpet hemocyanin round window immunization. Audiol. Med. 5, 182−187.

Zou, J., Saulnier, P., Perrier, T., Zhang, Y., Manninen, T., Toppila, E., et al., 2008. Distribution of lipid nanocapsules in different cochlear cell populations after round window membrane permeation. J. Biomed. Mater. Res. B Appl. Biomater. 87 (1), 10−18.

Zou, J., Poe, D., Bjelke, B., Pyykko, I., 2009. Visualization of inner ear disorders with MRI in vivo: from animal models to human application. Acta Otolaryngol. Suppl. 560, 22−31.

Zou, J., Zhang, Y., Zhang, W., Ranjan, S., Sood, R., Mikhailov, A., et al., 2009. Internalization of liposome nanoparticles functionalized with TrkB ligand in rat cochlear cell populations. Eur. J. Nanomedicine 3, 8−14.

Zou, J., Zhang, W., Poe, D., Zhang, Y., Ramadan, U.A., Pyykko, I., 2010. Differential passage of gadolinium through the mouse inner ear barriers evaluated with 4.7T MRI. Hear Res. 259 (1−2), 36−43.

Zou, J., Ramadan, U.A., Pyykko, I., 2010. Gadolinium uptake in the rat inner ear perilymph evaluated with 4.7 T MRI: a comparison between transtympanic injection and gelatin sponge-based diffusion through the round window membrane. Otol. Neurotol. 31 (4), 637−641.

Zou, J., Zhang, W., Poe, D., Qin, J., Fornara, A., Zhang, Y., et al., 2010. MRI manifestation of novel superparamagnetic iron oxide nanoparticles in the rat inner ear. Nanomedicine (Lond) 5 (5), 739−754.

Zou, J., Sood, R., Ranjan, S., Poe, D., Ramadan, U.A., Kinnunen, P.K., et al., 2010. Manufacturing and in vivo inner ear visualization of MRI traceable liposome nanoparticles encapsulating gadolinium. J. Nanobiotechnology 8, 32.

Zou, J., Yoshida, T., Ramadan, U.A., Pyykko, I., 2011. Dynamic enhancement of the rat inner ear after ultra-small-volume administration of Gd-DOTA to the medial wall of the middle ear cavity. ORL J. Otorhinolaryngol. Relat. Spec. 73 (5), 275−281.

Zou, J., Li, M., Zhang, Y., Zheng, G., Chen, D., Chen, S., et al., 2011. Transport augmentation through the blood-inner ear barriers of Guinea pigs treated with 3-nitropropionic acid and patients with acute hearing loss, visualized with 3.0 T MRI. Otol. Neurotol. 32 (2), 204−212.

Zou, J., Poe, D., Ramadan, U.A., Pyykko, I., 2012. Oval window transport of Gd-dOTA from rat middle ear to vestibulum and scala vestibuli visualized by in vivo magnetic resonance imaging. Ann. Otol. Rhinol. Laryngol. 121 (2), 119−128.

Zou, J., Sood, R., Ranjan, S., Poe, D., Ramadan, U.A., Pyykko, I., et al., 2012. Size-dependent passage of liposome nanocarriers with preserved post-transport integrity across the middle-inner ear barriers in rats. Otol. Neurotol. 33 (4), 666−673.

Zou, J., Sood, R., Zhang, Y., Kinnunen, P.K., Pyykko, I., 2014. Pathway and morphological transformation of liposome nanocarriers after release from a novel sustained inner-ear delivery system. Nanomedicine (Lond) 9 (14), 2143−2155.

Zou, J., Feng, H., Mannerstrom, M., Heinonen, T., Pyykko, I., 2014. Toxicity of silver nanoparticle in rat ear and BALB/c 3T3 cell line. J. Nanobiotechnology 12, 52.

Zou, J., Hannula, M., Misra, S., Feng, H., Labrador, R.H., Aula, A.S., et al., 2015. Micro CT visualization of silver nanoparticles in the middle and inner ear of rat and transportation pathway after transtympanic injection. J. Nanobiotechnology 13, 5.

Zou, J., Koivisto, J., Lahelma, J., Aarnisalo, A., Wolff, J., Pyykko, I., 2015. Imaging optimization of temporal bones with cochlear implant using a high-resolution cone beam CT and the corresponding effective dose. Ann. Otol. Rhinol. Laryngol. 124 (6), 466−473.

Zou, J., Hannula, M., Lehto, K., Feng, H., Lahelma, J., Aula, A.S., et al., 2015. X-ray microtomographic confirmation of the reliability of CBCT in identifying the scalar location of cochlear implant electrode after round window insertion. Hear Res. 326, 59−65.

Zou, J., Ostrovsky, S., Israel, L.L., Feng, H., Kettunen, M.I., Lellouche, J.M., et al., May 30, 2016a. Efficient penetration of ceric ammonium nitrate oxidant-stabilized gamma-maghemite nanoparticles through the oval and round windows into the rat inner ear as demonstrated by MRI. J. Biomed. Mater Res. B Appl. Biomater. http://dx.doi.org/10.1002/jbm.b.33719 [Epub ahead of print].

Zou, J., Feng, H., Zhang, Y., Zhang, W., Pyykko, I., 2016. Intratympanic Delivery of Nanomaterials for the Inner Ear and the Associated Pathway and Safety. European & Global Summit for Cutting-Edge Medicine; June 26−19. CLINAM, Basel, Switzerland.

Zou, J., Isomäki, A., Hirvonen, T., Arnisalo, A., Jero, J., Pyykko, I., 2016. Label-free visualization of cholesteatoma in the mastoid and tympanic membrane using CARS microscopy. J. Otol. 11, 127−133.